Electronic Supplementary Information (ESI):

Blue-Emitting NH_4^+-Doped $MAPbBr_3$ Perovskite Quantum Dots with Nearly Unit Quantum Yield and Super Stability

Jidong Deng, Jiao Xun, Youcheng Qin, Ming Li and Rongxing He*

Key Laboratory of Luminescence Analysis and Molecular Sensing, Ministry of Education, College of Chemistry and Chemical Engineering, Southwest University, Chongqing 400715, China.

*Corresponding author: herx@swu.edu.cn

Materials.

All materials were used without purification unless otherwise specified. Lead (II) bromide ($PbBr_2$, 99.999%, Alfa Aesar), Lead(II) chloride ($PbCl_2$, 99.99%, Aladdin), ammonium bromide (NH_4Br, 99.99%; Aladdin), ammonium chloride (NH_4Cl, 99.90%; Cologne, chengdu), Formamidinium Bromide (FABr, 99.50%, Maituowei, Shanghai), methylamine (CH_3NH_2, 33 wt % in absolute ethanol, Aladdin), HBr (48 wt% in water, Aladdin), HCl (48 wt% in water, Aladdin), oleic acid (OA, Alfa) Aesar, tech, 90%), n-Octylamine (OCTAm, approximate C18 content 80-90%, Aladdin), Dimethylsulfoxide (DMSO, 99.8%, Aladdin), N, N-dimethylformamide (DMF, 99.9%, Aladdin) were purchased from Sigma-Aldrich.

The synthesis of CH_3NH_3X (X=Br, Cl).

CH_3NH_3Br (MABr) was synthesized by the dropwise addition of hydrobromic acid (HBr) to a methylamine solution in an ice bath. According to the previous reports, 24 mL of methylamine solution was stirred under the ice-water bath, then 10 mL of HBr

acid was dropped into methylamine solution. The ice-cold solution was stirred for 2 h followed by the solvent evaporation using a rotary evaporator (95 mbar vacuum, 400 r.p.m. rotation) at 60 °C. The resulting white product was dissolved in ethanol and recrystallized using diethyl ether. The fresh white crystals were washed three times using diethyl ether and then dried in vacuum for 24 h. For the synthesis of CH_3NH_3Cl (MACl), the same method was used.

The synthesis of $MA_{1-x}(NH_4)_xPbBr_3$ QDs and $FA_{1-x}(NH_4)_xPbBr_3$ QDs.

For example, the synthesis of $MAPbBr_3$ QDs was carried out at room temperature using the modified LARP approach,[1] by injecting 0.2 mL of precursor mixture (we further express it in a general term "precursor") into a “bad solvent” toluene (10 mL) under vigorous stirring. Specifically, the precursor was prepared by mixing 0.1 mmol CH_3NH_3Br prepared above, 0.1 mmol $PbBr_2$, oleic acid (OA)/n-Octylamine (OCTAm) mixture by volume(OA/Octyl amine=15:1) dissolved in 2 mL “good solvent” DMSO or DMF, respectively. For the synthesis of $MA_{1-x}(NH_4)_xPbBr_3$ (x=0.0-0.9) QDs, according to the above method, only the molar ratio of MABr/NH_4Br is changed. The above perovskite QDs original solution was centrifuged (8000 rpm, 5 minutes), then the supernatant was discarded and the precipitate was redispersed in toluene. Finally, the QDs were centrifuged (5000 rpm, 5 minutes) again.

Due to the different solubility, in the synthesis of $MA_{1-x}(NH_4)_xPbCl_3$ (x=0.0-0.9) QDs, according to the above method, only the molar ratio of MABr/NH_4Cl is changed, and the chemicals were dissolved in the mixture solution of 2 mL DMSO and DMF.

Characterization

Transmission electron microscope (TEM) images were obtained using the Talos F200X microscope. HRTEM images were measured on FEI Tecnai G20. The XRD patterns were performed using the Shimadzu-7000 diffractometer with Cu Kα (λ = 1.5406 Å) radiation. The UV-Vis absorption spectra were obtained using a Shimadzu 3600 UV-Vis spectrophotometer. The photoluminescence (PL) spectra and the time-corrected single-photon-counting (TCSPC) PL decay were measured by Florolog-3 fluorescence spectrometer (Horiba, USA) (the excited wavelength was 360 nm). The photoluminescence quantum yield (PLQY) was measured by C9920-02 (Hamamatsu photonics K.K., Japan). According to the method reported by Prato *et al*,[2] the calculation of PLQY was:

$$PLQY(\%) = \frac{SEM - BEM}{BEX - SEX} \times 100$$

SEM is the sample emission, which collects the photons emitted by the sample, BEM denotes the blank emission, which is a measurement value performed with the cuvette containing only the solvent (blank) in the same spectral range used for the SEM, SEX is the sample excitation to record the photons at the pumping wavelength that are not absorbed by the sample, and BEX is the blank excitation to record the photons at the pumping wavelength going through the blank. Any reabsorption correction factor was neglected in PLQY calculations, since the solutions investigated were diluted to the point that reabsorption of the PL could be neglected.

Transient absorption:

Under ambient conditions, the fs-TA measurements were performed on a Helios pump-probe system (Ultrafast Systems LLC) combined with an amplified

femtosecond laser system (Coherent).[3] Optical parametric amplifier (TOPAS-800-fs) provided a 400 nm pump pulse (~20 nJ/pulse at the sample, corresponding to a pump fluence of ~168 uJ/cm^2 given the typical focus radii of ~150 μm)), which was excited by a Ti: sapphire regenerative amplifier (Legend Elite-1K-HE; 800 nm), 35 fs, 7 mJ/pulse, 1 kHz) and seeded with a mode-locked Ti: sapphire laser system (Micra 5) and an Nd: YLF laser (EvolutIon 30) pumped. Focusing the 800 nm beams (split from the regenerative amplifier with a tiny portion, ~400 nJ/pulse) onto a sapphire plate produced the white-light continuum (WLC) probe pulses (420-760 nm). The pulse-to-pulse fluctuation of the WLC is corrected by a reference beam split from WLC. A motorized optical delay line was used to change the time delays (0-8 ns) between the pump and probe pulses. The instrument response function (IRF) was determined to be ~100 fs by a routine cross-correlation procedure. A mechanical chopper operated at a frequency of 500 Hz used to modulate the pump pulses such that the fs-TA spectra with and without the pump pulses can be recorded alternately. The temporal and spectral profiles (chirp-corrected) of the pump-induced differential transmission of the WLC probe light (i.e., absorbance change) were visualized by an optical fiber-coupled multichannel spectrometer (with a CMOS sensor) and further processed by the Surface Xplorer software.

DFT Calculation.

The first-principle calculations were performed using the Vienna *Ab-initio* Simulation Package (VASP) based on the projector augmented wave (PAW) method with a cutoff energy of 400 eV.[4, 5] The generalized gradient approximation (GGA)[6]

with the Perdew-Burke-Ernzerhof (PBE)[7] functional was used to describe the electron exchange-correlation interactions. The structural optimization was carried out until the force tolerance on each atom was smaller than 0.02 eV/Å. The total energy was converged to 10^{-5} eV. For k-point integration within the first Brillouin zone, a 3×3×5 Monkhorst-Pack grid for a 2×2×1 supercell was selected. To get a comprehensive understanding, there are two calculated models for $MA_{1-x}(NH_4)_xPbBr_3$ (x=0.0-0.9) QDs: the first model is that the MA^+ ions in the cell edge center are replaced by NH_4^+ ions, and the second one is that the MA^+ ions at the cell vertex and face center are replaced. The optimized structures were shown in Fig. S14.

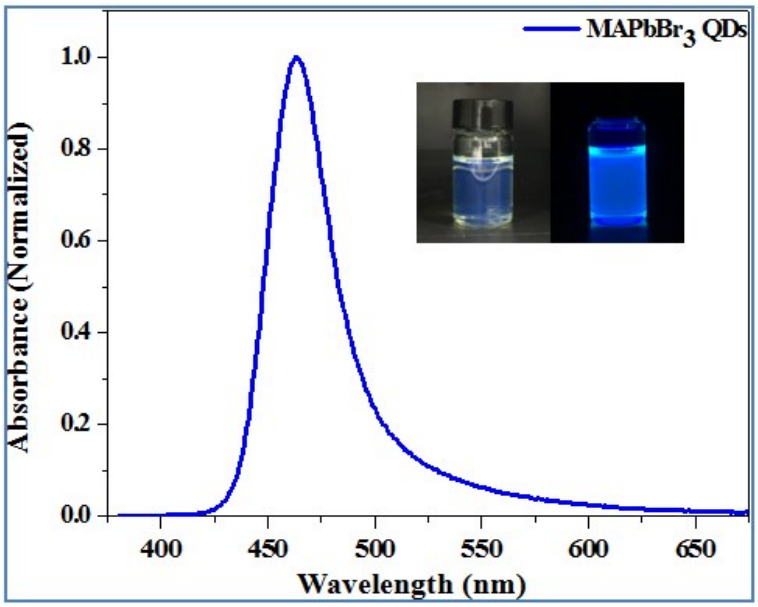

Fig. S1 The normalized PL of the fresh $MAPbBr_3$ QDs. Insert: photographs of the as-obtained colloidal $MAPbBr_3$ QDs (left: under fluorescent lamp; right: under 365 nm UV light). Note that the freshly prepared $MAPbBr_3$ QDs will change rapidly from blue to green in about 15 minutes (as shown in the first digital photo of Fig. 1a).

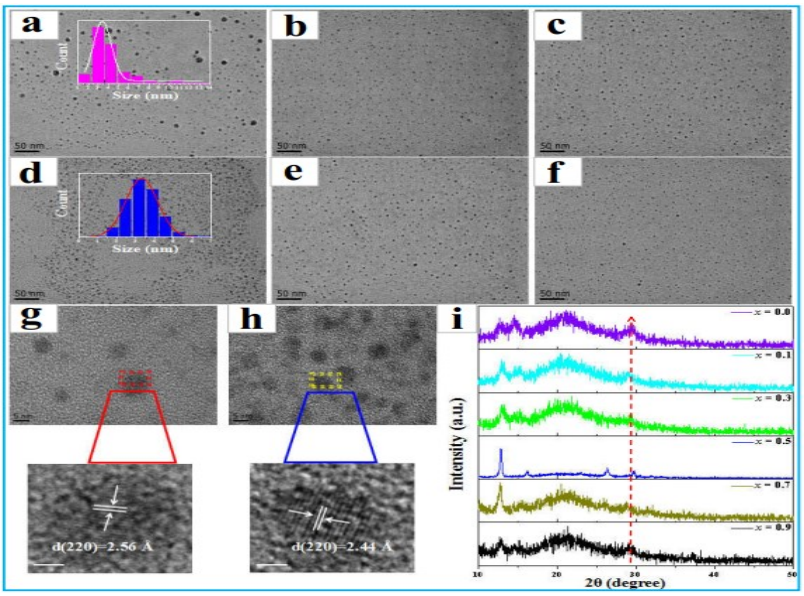

Fig. S2 (a-f) TEM images of $MA_{1-x}(NH_4)_xPbBr_3$ QDs (x=0.0, 0.1, 0.3, 0.5, 0.7, 0.9). The insets in (a, d) show size distribution histograms for x=0.0 and x=0.5. (g, h) high-resolution TEM images of x=0.0 and x=0.5, respectively. (i) XRD patterns of $MA_{1-x}(NH_4)_xPbBr_3$ QDs with different x value.

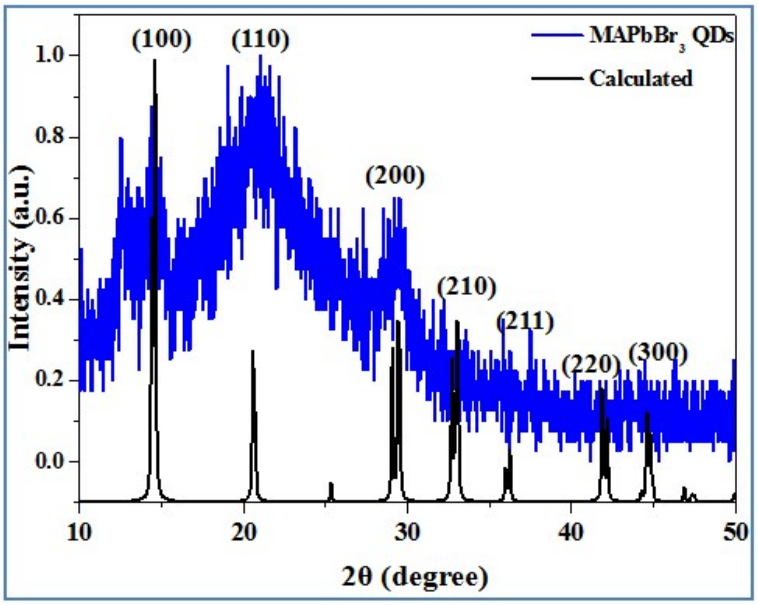

Fig. S3 XRD patterns of $MAPbBr_3$.

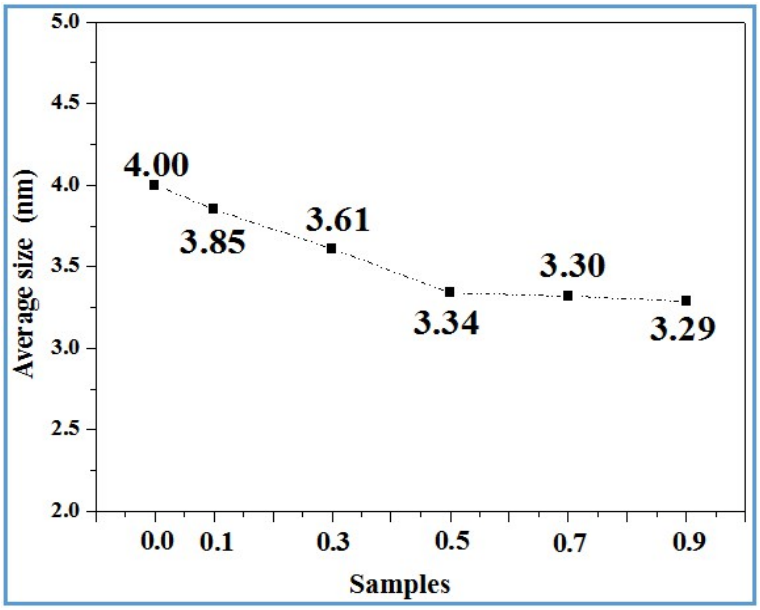

Fig. S4 Variation of average sizes of $MA_{1-x}(NH_4)_xPbBr_3$ (x=0.0-0.9) QDs.

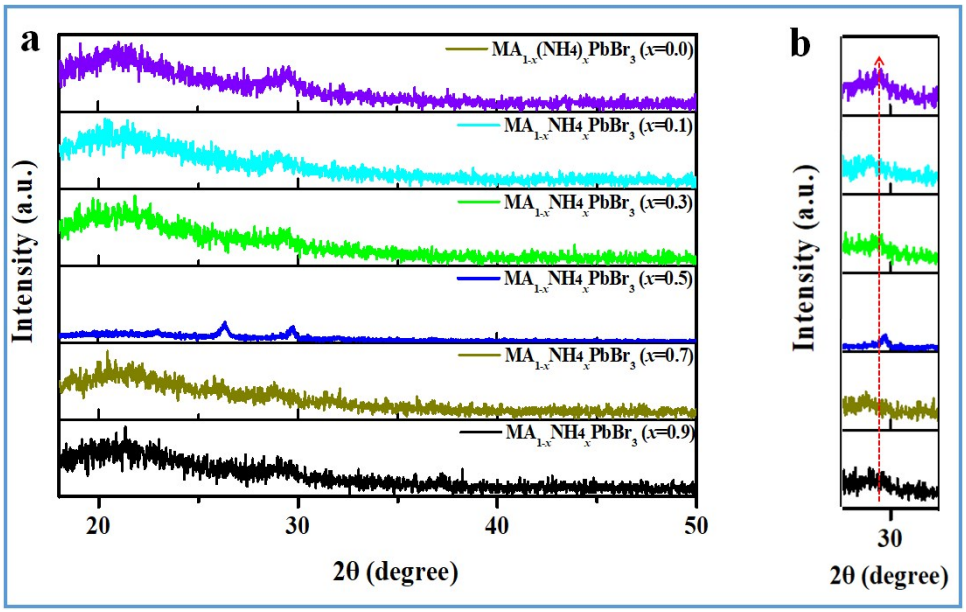

Fig. S5 (a) XRD patterns of $MA_{1-x}(NH_4)_xPbBr_3$ (x=0.0-0.9) perovskite QDs with different x value. (b) The enlarged XRD profiles of the $MA_{1-x}(NH_4)_xPbBr_3$ QDs when diffraction angle is about 30°.

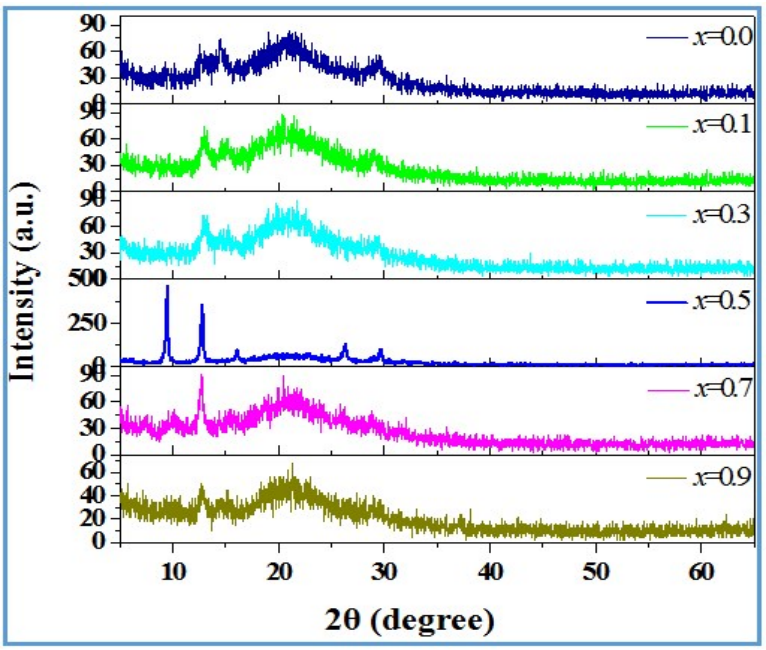

Fig. S6 Intensity of XRD spectra of the $MA_{1-x}(NH_4)_xPbBr_3$ (x=0.0-0.9) QDs.

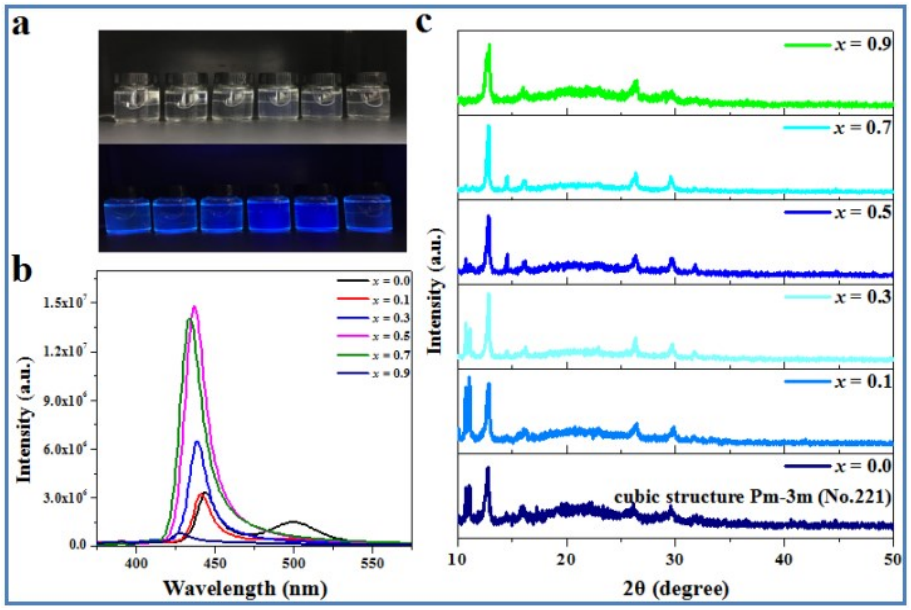

Fig. S7 (a) The optical images of colloidal $FA_{1-x}(NH_4)_xPbBr_3$ (x=0.0-0.9) QDs solution under 365 nm UV light. (b) Intensities of PL spectra of $FA_{1-x}(NH_4)_xPbBr_3$ (x=0.0-0.9) QDs. (c) The XRD patterns of $FA_{1-x}(NH_4)_xPbBr_3$ (x=0.0-0.9) QDs. Notes: for the structural analysis, considering that the absence of any $FAPbX_3$ (X=Cl, Br, I) reference patterns in the ICSD database, the XRD patterns of our $FAPbBr_3$ QDs is compared with that of the cubic structure reported by Maksym V. Kovalenko *et al*.[8]

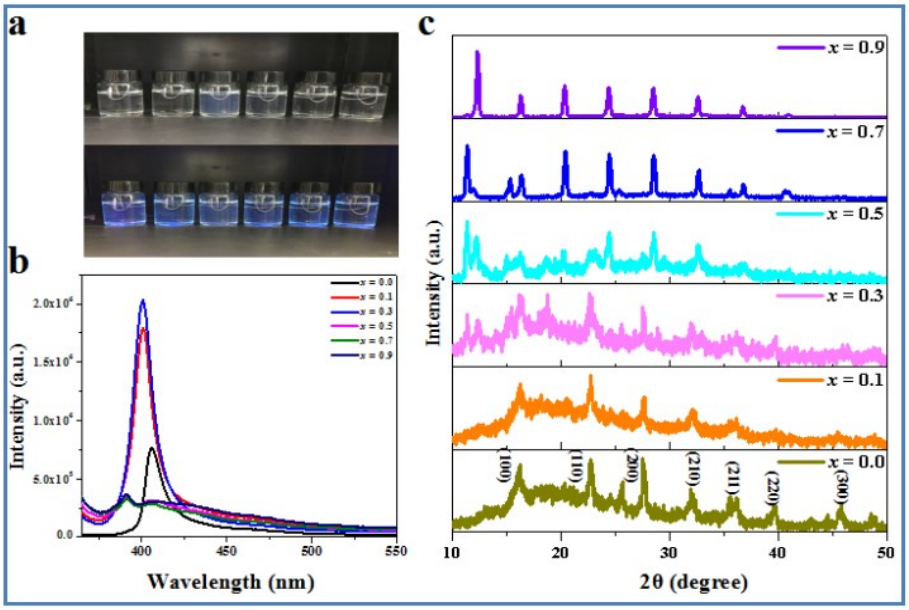

Fig. S8 (a) The optical images of colloidal $MA_{1-x}(NH_4)_xPbCl_3$ (x=0.0-0.9) QDs solution under 365 nm UV light. (b) Intensities of the PL spectra of $MA_{1-x}(NH_4)_xPbCl_3$ (x=0.0-0.9) QDs. (c) The XRD spectra of $MA_{1-x}(NH_4)_xPbCl_3$ (x=0.0-0.9) QDs.

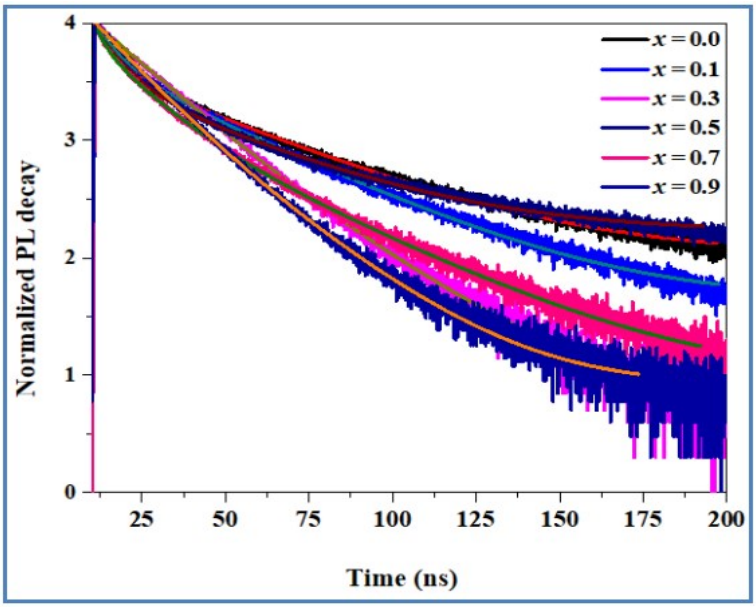

Fig. S9 PL lifetime of $MA_{1-x}(NH_4)_xPbBr_3$ (x=0.0-0.9) QDs.

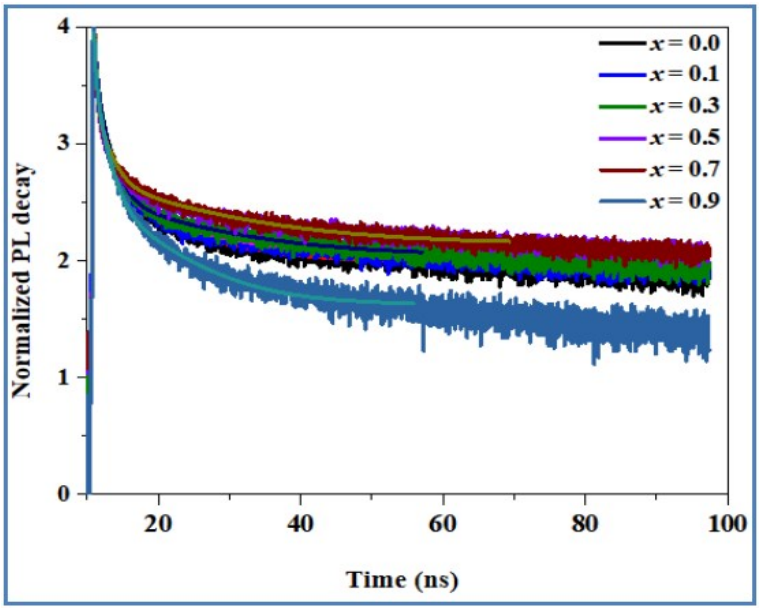

Fig. S10 PL lifetime of $FA_{1-x}(NH_4)_xPbBr_3$ (x=0.0-0.9) QDs.

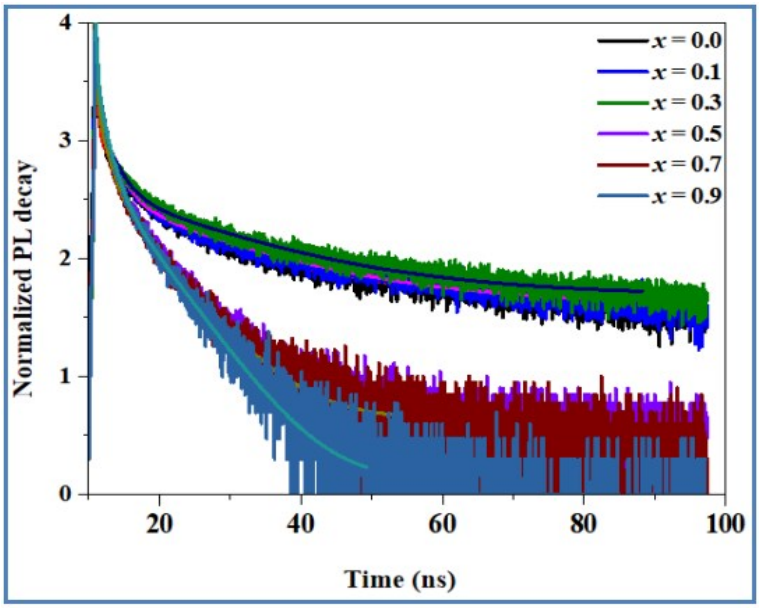

Fig. S11 PL lifetime of $MA_{1-x}(NH_4)_xPbCl_3$ (x=0.0-0.9) QDs.

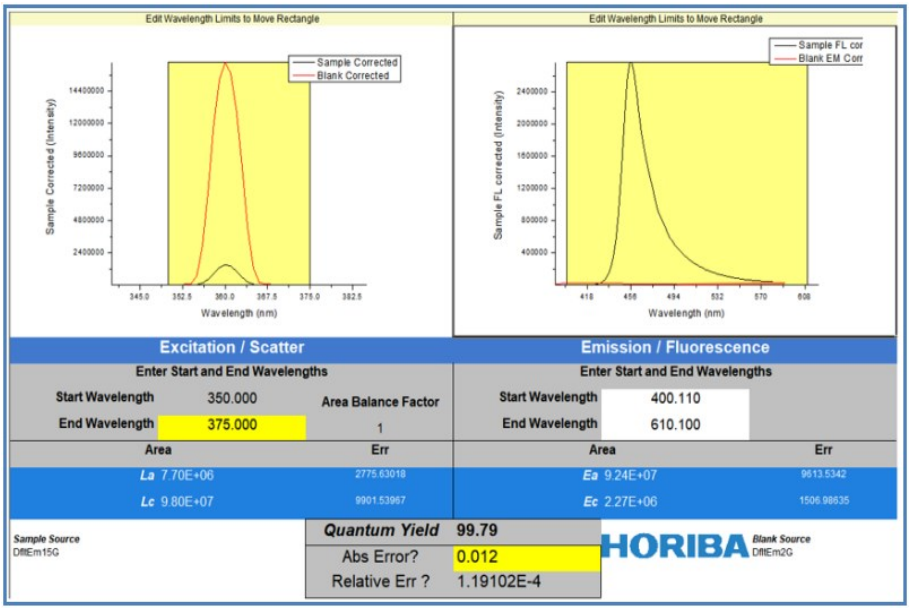

Fig. S12 PLQY measurements result of $MA_{0.5}(NH_4)_{0.5}PbBr_3$ QDs colloidal solution.

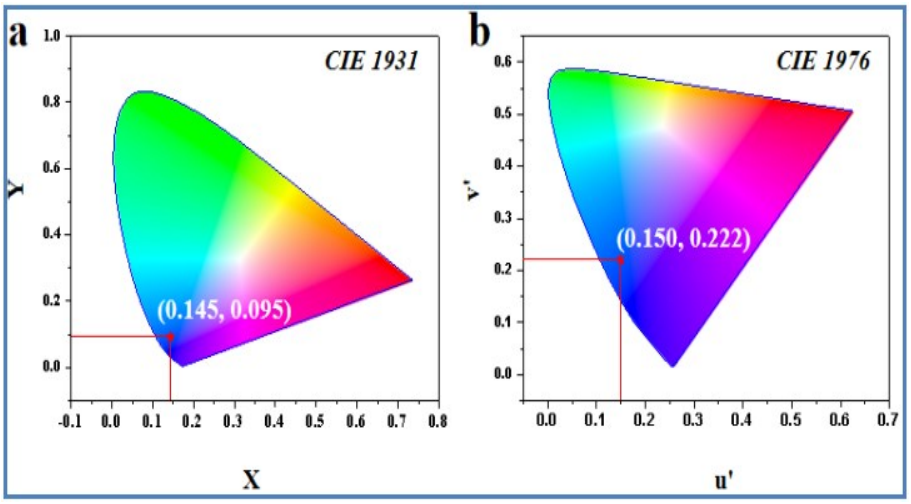

Fig. S13 The CIE coordinates for $MA_{0.5}(NH_4)_{0.5}PbBr_3$ QDs: (a) CIE 1931; (b) CIE 1976.

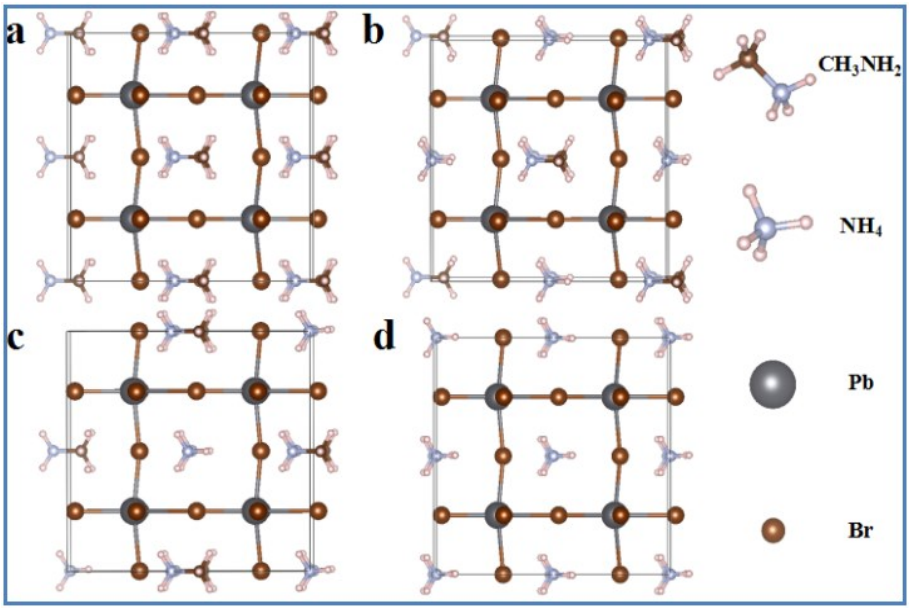

Fig. S14 DFT optimized structures: (a) $MAPbBr_3$. (b) $MA_{0.5}(NH_4)_{0.5}PbBr_3$ (MA^+ ions in the edge center are replaced by NH_4^+). (c) $MA_{0.5}(NH_4)_{0.5}PbBr_3$ (MA^+ ions at the vertex and the face center are substituted). (d) NH_4PbBr_3.

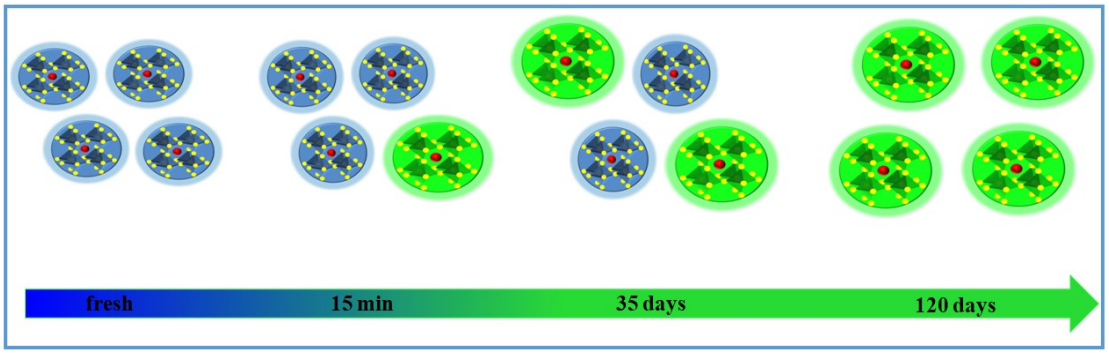

Fig. S15 Schematic illustration of the morphology evolution and growth mechanism for undoped blue $MAPbBr_3$ QDs.

Table S1. Fitted PL lifetime of $MA_{1-x}(NH_4)_xPbBr_3$ (x=0.0-0.9) QDs (by bi-exponential decay).

$MA_{1-x}(NH_4)_xPbBr_3$ QDs	τ_1 (ns)	τ_2 (ns)	τ_{ave} (ns)	Em-Wavelength (nm)	FWHM (nm)	PLQY (100%)	Γ_{rad} μs^{-1}	$\Gamma_{non\text{-}rad}$ μs^{-1}
x=0.0	7.400	34.97	17.60	456 and 530	--	86.9	49.375	7.443
x=0.1	7.813	36.93	18.01	455 and 528	--	88.6	49.195	6.329
x=0.3	17.07	32.77	18.56	455 and 527	--	92.5	49.838	4.041
x=0.5	7.990	34.00	19.94	448	28	99.79	50.045	0.105
x=0.7	12.74	23.07	15.45	437	19	65.2	42.201	22.52
x=0.9	12.94	21.67	14.03	437	16	46.3	33.001	38.27

Notes: using the values of PLQY and average lifetimes, we can evaluate the radiative and non-radiative decay rates of these QDs based on the following equations[9]:

$$\Gamma_{rad} = \frac{PLQY}{\tau_{ave}} \qquad (1)$$

$$\Gamma_{non\text{-}rad} = \frac{1}{\tau_{ave}} - \Gamma_{rad} = \frac{1 - PLQY}{\tau_{ave}} \qquad (2)$$

where Γ_{rad} and $\Gamma_{non-rad}$ are the radiative and non-radiative recombination rates, respectively, and τ_{ave} is the average lifetime of the samples.

Table S2. Fitted PL lifetime of $FA_{1-x}(NH_4)_xPbBr_3$ (x=0.0-0.9) QDs (by three exponential fitting).

$FA_{1-x}(NH_4)_xPbBr_3$ QDs	τ_1 (ns)	τ_2 (ns)	τ_3 (ns)	τ_{ave} (ns)	Em-Wavelength (nm)	FWHM (nm)
x=0.0	1.487	9.961	2.910	0.836	443 and 500	--
x=0.1	1.309	9.258	0.251	0.858	440 and 498	--
x=0.3	14.23	1.546	0.331	0.973	438	14
x=0.5	12.73	1.491	0.255	8.023	437	17
x=0.7	1.596	15.38	0.254	1.066	433	17
x=0.9	1.298	7.980	0.239	0.841	427	18

Table S3. Fitted PL lifetime of $MA_{1-x}(NH_4)_xPbCl_3$ (x=0.0-0.9) QDs (by three exponential fitting).

$MA_{1-x}(NH_4)_xPbCl_3$ QDs	τ_1 (ns)	τ_2 (ns)	τ_3 (ns)	τ_{ave} (ns)	Em-Wavelength (nm)	FWHM (nm)
x=0.0	14.89	2.475	0.209	0.803	406	12
x=0.1	2.159	17.14	0.227	1.064	401	13
x=0.3	2.061	17.88	0.221	1.164	400	13
x=0.5	7.803	1.867	0.215	0.714	391	--
x=0.7	1.375	6.222	0.183	0.679	391	--
x=0.9	1.267	5.411	0.217	0.608	390	--

Table S4. Optical parameter comparison of halide perovskite QDs.

Materials	Emission wavelength (nm)	Synthetic temperature (℃)	Synthetic method	PLQY (%)	Stability	Ref
$CsPb_{0.93}Cu_{0.07}(Br/Cl)_3$ QDs	453	120	HI	80	250℃ (40%)^{TS}	Andrey L[10]
Sb^{3+}-doped $CsPbBr_3$ NCs	460	0	LARP	73.8	--	Xu[11]
Al^{3+}-doped $CsPbBr_3$ NCs	456	150	HI	32	100℃ (40%)^{TS}	Liu[12]
$CsPbBr_3$@Amorphous CsPbBrx QDs	452	160	HI	84	--	Wang[13]
$CsPbX_3$ QDs	455	20	LARP	37	--	Zeng[14]
$CsPbX_3$ QDs	442	RT	Tip-sonication	22	--	Tong[15]
$CsPbX_3$ NCs	450	160	HI	50	35days (20%)^{ES}	Huang[16]
$CsPbBr_3$ NCs	460	140	HI	35	--	Pan[17]
$CsPbBr_3$ NCs	453	90	HI	50.41	100℃ (10%)^{ES}	Yu[18]
$CsPbBr_3$ NCs	452	143	HI	68	1h	Li[19]

					(90%)[ES]	
$CsPbBr_3$ NCs	457	-20	LARP	40.3	--	Deng[20]
$CsPbBr_3$ NCs	465	0	LARP	51.7	--	Deng[20]
$CH_3NH_3PbBr_3$ QDs	465	500	Mesoporous	1.2	--	Malgras[21]
$CH_3NH_3PbBr_3$ QDs	460	RT	Water-Oil	4	--	Li[22]
$CH_3NH_3PbBr_3$ QDs	475	0	LARP	74	--	Huang[23]
$MAPbBr_3$@PVA nanofibers	488	50	in-situ fabrication	49	--	Zhong[24]
$MAPbBr_3$	456	RT	LARP	86.9	15min	This work
$MA_{0.5}(NH_4)_{0.5}PbBr_3$ QDs	448	RT	LARP	99.79	120days (70%)[ES]	This work

Abbreviations: Full width at half maximum (FWHM); Ligand-assisted reprecipitation (LARP); Nanocrystals (NCs); Nanoplatelets (NPLs); Nanowires (NWs); Quantum dots (QDs); Photoluminescence quantum yields (PLQY); Hot injection (HI); Room temperature (RT); Thermal stability (TS); Emission stability (ES).

Table S5. Calculated formation energies of $MAPbBr_3$ QDs and $MA_{0.5}(NH_4)_{0.5}PbBr_3$ QDs, and the energy difference between them.

Crystal	Formation energy (eV)	ΔE (eV)
$MAPbBr_3$	-102.43	--
$MA_{0.5}(NH_4)_{0.5}PbBr_3$ (in the edge center)	-103.16	-0.73
$MA_{0.5}(NH_4)_{0.5}PbBr_3$ (at the vertex or the face center)	-103.43	-1.00
NH_4PbBr_3	-103.60	-1.17

Table S6. Comparison of optical parameters of $MA_{0.5}(NH_4)_{0.5}PbBr_3$ perovskite QDs before and after 120 days in the air.

$MA_{1-x}(NH_4)_xPbBr_3$ QDs (x=0.5)	Em-Wavelength (nm)	FWHM (nm)	PLQY (%)
fresh	448	28	99.79
After 120 days	451	35	75.8

References

1. F. Zhang, H. Zhong, C. Chen, X.-g. Wu, X. Hu, H. Huang, J. Han, B. Zou and Y. Dong, *ACS Nano*, 2015, **9**, 4533-4542.
2. Q. A. Akkerman, V. D'Innocenzo, S. Accornero, A. Scarpellini, A. Petrozza, M. Prato and L. Manna, *J. Am. Chem. Soc.*, 2015, **137**, 10276-10281.
3. H. Cho, J. S. Kim, C. Wolf, Y.-H. Kim, H. J. Yun, S.-H. Jeong, A. Sadhanala, V. Venugopalan, J. W. Choi and C.-L. Lee, *ACS nano*, 2018, **12**, 2883-2892.
4. G. Kresse and J. Furthmüller, *Comput. Mater. Sci.*, 1996, **6**, 15-50.
5. G. Kresse and J. Furthmüller, *Phys. Rev. B: Condens. Matter Mater. Phys.*, 1996, **54**, 11169-11186.
6. J. P. Perdew, K. Burke and M. Ernzerhof, *Phys. Rev. Lett.*, 1996, **77**, 3865-3868.
7. J. P. Perdew, M. Ernzerhof and K. Burke. *J. Chem. Phys.* 1996, **105**, 9982-9985.
8. L. Protesescu, S. Yakunin, M. I. Bodnarchuk, F. Bertolotti, N. Masciocchi, A. Guagliardi and M. V. Kovalenko, *J. Am. Chem. Soc.*, 2016, **138**, 14202-14205.
9. Z. J. Yong, S. Q. Guo, J. P. Ma, J. Y. Zhang, Z. Y. Li, Y. M. Chen, B. B. Zhang, Y. Zhou, J. Shu, J. L. Gu, L. R. Zheng, O. M. Bakr and H. T. Sun, *J Am Chem Soc*, 2018, **140**, 9942-9951.
10. C. Bi, S. Wang, Q. Li, S. V. Kershaw, J. Tian and A. L. Rogach, *J. Phys. Chem. Lett.*, 2019, **10**, 943-952.
11. Z. Liang, S. Zhao, Z. Xu, B. Qiao, P. Song, D. Gao and X. Xu, *ACS Appl. Mater. Interfaces.*, 2016, **8**, 28824-28830.
12. M. Liu, G. Zhong, Y. Yin, J. Miao, K. Li, C. Wang, X. Xu, C. Shen and H. Meng, *Adv. Sci.*, 2017, **4**, 1700335.
13. S. Wang, C. Bi, J. Yuan, L. Zhang and J. Tian, *ACS Energy Lett.*, 2017, **3**, 245-251.
14. X. Li, Y. Wu, S. Zhang, B. Cai, Y. Gu, J. Song and H. Zeng, Adv. Funct. Mater., 2016, **26**, 2435-2445.
15. Y. Tong, E. Bladt, M. F. Aygüler, A. Manzi, K. Z. Milowska, V. A. Hintermayr, P. Docampo, S. Bals, A. S. Urban and L. Polavarapu, *Angew. Chem. Int. Ed.*, 2016, **55**, 13887-13892.
16. S. Wei, Y. Yang, X. Kang, L. Wang, L. Huang and D. Pan, *Chem. Commun.*, 2016, **52**, 7265-7268.
17. A. Pan, B. He, X. Fan, Z. Liu, J. J. Urban, A. P. Alivisatos, L. He and Y. Liu, *ACS nano*, 2016, **10**, 7943-7954.
18. X. Zhang, H. Wang, Y. Hu, Y. Pei, S. Wang, Z. Shi, V. L. Colvin, S. Wang, Y. Zhang and W. W. Yu, *J. Phys. Chem. Lett*., 2019, **10**, 1750-1756.
19. J. Li, L. Gan, Z. Fang, H. He and Z. Ye, *J. Phys. Chem. Lett.*, 2017, **8**, 6002-6008.
20. S. Sun, D. Yuan, Y. Xu, A. Wang and Z. Deng, *ACS nano*, 2016, **10**, 3648-3657.
21. V. Malgras, S. Tominaka, J. W. Ryan, J. Henzie, T. Takei, K. Ohara and Y. Yamauchi, *J. Am. Chem. Soc.*, 2016, **138**, 13874-13881.
22. F. Li, L. Cao, S. Shi, H. Gao, L. Song, C. Geng, W. Bi and S. Xu, *Angew. Chem. Int. Ed.*, 2019, **58**, 17631.
23. H. Huang, A. S. Susha, S. V. Kershaw, T. F. Hung and A. L. Rogach, *Adv. Sci.*, 2015, **2**, 1500194.
24. L. Meng, C. Yang, J. Meng, Y. Wang, Y. Ge, Z. Shao, G. Zhang, A. L. Rogach and H. Zhong, *Nano Research*, 2019, **12**, 1411-1416.